Density Functional Theory Calculations of the Molecular Force Field of L-Ascorbic Acid, Vitamin C

Laura C. Bichara,[†] Hernán E. Lanús,[†] Carlos G. Nieto,[‡] and Silvia A. Brandán*,[†]

Cátedra de Fisicoquímica I, Instituto de Química Física, Facultad de Bioquímica, Química y Farmacia, Universidad Nacional de Tucumán, San Lorenzo 456, T4000CAN, S. M. de Tucumán, R, Argentina and Cátedra de Microbiología General, Instituto de Microbiología, Facultad de Bioquímica, Química y Farmacia, Universidad Nacional de Tucumán, Ayacucho 471, T4000CAN, S. M. de Tucumán, R, Argentina

Received: December 30, 2009; Revised Manuscript Received: March 4, 2010

We have studied L-ascorbic acid and characterized it by infrared spectroscopy in solid and aqueous solution phases. The density functional theory (DFT) method together with Pople's basis set show that three stable molecules for the compound have been theoretically determined in the gas phase, and that an average of only two more stable conformations are present in the solid phase, as it was experimentally observed. The harmonic vibrational wavenumbers for the optimized geometries of both structures were calculated at B3LYP/6-31G*and B3LYP/6-311++G** levels at the proximity of the isolated molecule. For a complete assignment of the vibrational spectra in the compound solid and aqueous solution phases, DFT calculations were combined with Pulay's scaled quantum mechanics force field methodology in order to fit the theoretical wavenumber values to the experimental ones. In this way, a complete assignment of all the observed bands in the infrared spectrum for L-ascorbic acid was performed. The natural bond orbital study reveals the characteristics of the electronic delocalization of the three structures while the corresponding topological properties of electronic charge density are analyzed by employing Bader's atoms-in-molecules theory.

1. Introduction

The structure and spectroscopic property studies of L-ascorbic acid (vitamin C) is of great chemical, biochemical, and mainly pharmacological importance because the human body cannot produce vitamin C by itself.[1] This acid is required in the synthesis of many biological processes and must be ingested every day through citrus fruits, green leafy vegetables, or pharmaceutical products. The crystal and molecular structure of L-ascorbic acid has been determined by means of X-ray reflections[2] and neutron diffraction analysis.[3] Only the main characteristics of the vibrational spectra in the 4000−900 cm^{-1} region were published by Hvoslef and Klaeboe,[4] who have registered the infrared spectrum of the L-ascorbic acid in the solid phase and the corresponding Raman spectrum in aqueous solution. In another study, Panicker et al.[5] have recorded and analyzed the FT-IR, FT-Raman, and SERS spectra of vitamin C, and they have only assigned some of the molecule main bands related to the lactone ring. Ascorbic acid in dimethyl and diethylsulfoxide solutions has been recently studied by using vibrational spectroscopy.[6] The L-ascorbic acid has a high reactivity that makes the storage in the liquid and solid phases difficult due to the presence of an endiol group in its structure that gives it a high biological activity and powerful reducing properties. Thus, the degradation of ascorbic acid is related to juice flavor and color changes; for this reason, it is very important in nutrition. Moreover, a complete vibrational characterization of L-ascorbic acid is very important to know the decomposition degree of it and to quantify vitamin C in food and pharmaceutical products.[7] So far, there is no theoretical study concerning either geometry or vibrational spectra for this compound. To study the theoretical structure and carry out its complete assignment, a comparative work to evaluate the theory level and basis set that reproduce the existent experimental data for L-ascorbic acid was performed. For this purpose, the optimized geometries and frequencies for the normal vibration modes, considering three different structures (**A**, **B**, and **C** molecules) for L-ascorbic acid, which have marked differences in the orientations of their alcoholic hydrogen atoms, were calculated. Only the theoretical **A** and **B** structures are experimentally observed in the crystalline solid. Thus, for a complete and reliable compound assignment, the DFT calculations for both stable structures were combined with the scaled quantum mechanic force field (SQMFF) methodology[8−10] in order to fit the theoretical frequency values to the experimental one. In this paper, we have demonstrated that a molecular force field for L-ascorbic acid, calculated by using the B3LYP/6-31G* combination is well represented. DFT normal mode assignments, in terms of the potential energy distribution, are in agreement with those obtained from the normal coordinate analysis. In addition, the electronic properties of the three structures of the compound were evaluated by means of natural bond order (NBO)[11−14] and atoms-in-molecules (AIM)[15,16] studies in order to justify why the **C** structure cannot be experimentally seen.

2. Experimental Methods

A pure anhydrous Mallinckrodt commercial sample of L-ascorbic acid (**LAA**) was used. The IR spectrum of the solid substance in KBr pellets was recorded in the wavenumbers range from 4000 to 400 cm^{-1} with an FT-IR Perkin-Elmer spectrophotometer, provided with a Globar source and DGTS detector. The corresponding spectrum in aqueous solution was recorded between AgCl windows from 4000 to 400 cm^{-1} on the same

* To whom correspondence should be addressed. Phone: 54-381-4311044. Fax: +54-381-4248169. E-mail: sbrandan@fbqf.unt.edu.ar.
† Cátedra de Fisicoquímica I, Instituto de Química Física.
‡ Cátedra de Microbiología General, Instituto de Microbiología.

10.1021/jp912251g
Published on Web 03/18/2010

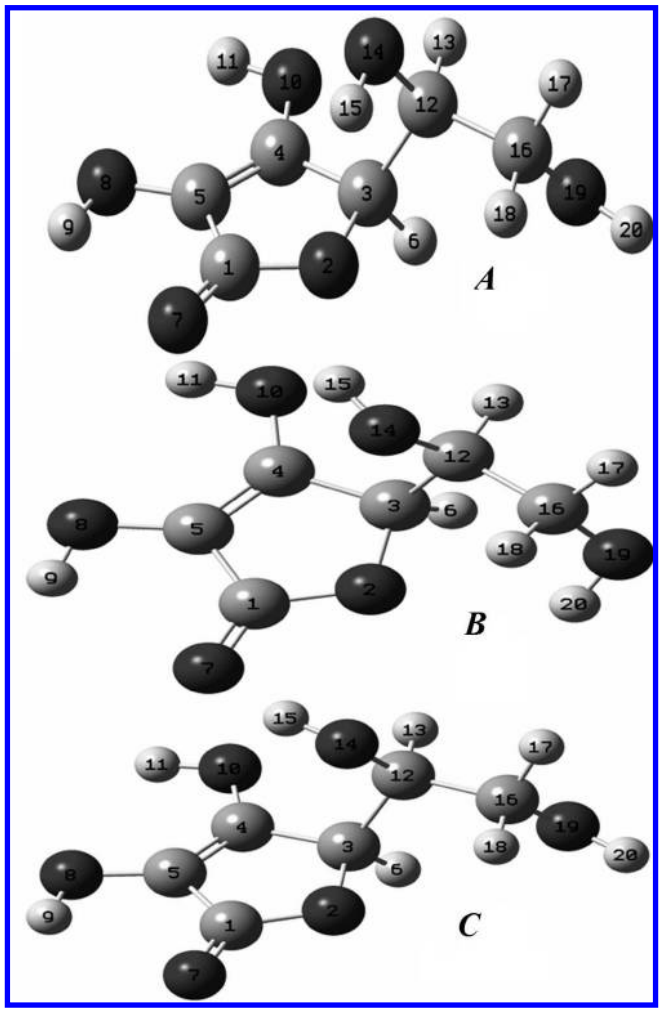

Figure 1. Theoretical structures **A**, **B**, and **C** and atoms numbering of L-ascorbic acid.

equipment. The Raman spectrum of L-ascorbic acid was taken from a previous study as reported in ref 4.

3. Computational Details

The potential energy curves associated with rotation around the C12−C16−O19-H20 and C3−C12−O14-H15 dihedral angles for the compound were studied at the B3LYP/6-31G* level. In both cases, three different stable conformations with geometry C_1 were obtained according to the position of alcoholic hydrogen atoms. The atom corresponding structures and labeling can be seen in Figure 1. The compound structures were fully optimized by using the hybrid B3LYP method,[17,18] as implemented in the GAUSSIAN 03 program,[19] with the 6-31G* and 6-311++G** basis sets being used. Atomic partial charges were also calculated for both structures from the electrostatic surface potential (ESP) according to the Merz−Singh−Kollman scheme[20] at the same level theory. The electronic charge density topological analysis was performed for all structures by using the AIM methodology,[15] and the AIM200 program package.[16] The NBO calculation was performed by using the NBO 3.1[11−14] program, as implemented in the GAUSSIAN 03 package.[19] The harmonic wavenumbers and the valence force field in Cartesian coordinates were calculated at the B3LYP/6-31G* and 6-311++G** approximation levels. The resulting force fields were transformed to "natural" internal coordinates by using the MOLVIB program.[21,22] The natural internal coordinates for the compound have been defined as proposed by Fogarasi et al.[23] while the ring coordinates were defined by Pulay et al.[24−26] and are listed in Table S1 of the Supporting Information. Following the SQMFF procedure,[8−10] the harmonic force field for all structures of this compound were evaluated at B3LYP/6-31G* level. The potential energy distribution components (PEDs) higher than or equal to 10% are subsequently calculated with the resulting SQM. The dimer species, with one unit of the **A** and **B** structures linked (Figure 2), was optimized at B3LYP/6-31G* calculation and then, at this same level of theory, a vibrational analysis was performed. The nature of all the vibration modes was carried out by means of the GaussView program.[27] The total energy for the dimer species by using the 6-31G* basis set was corrected for basis set superposition error (BSSE) by the standard Boys−Bernardi counterpoise method.[28]

4. Results and Discussion

4.1. Geometry Optimization. The potential energy curve associated with the rotation around the C12−C16−O19-H20 and C3−C12−O14-H15 dihedral angles for the molecule has been studied by using the B3LYP method with the 6-31G* and 6-311++G** basis sets, presenting in both cases three stable structures (**A**, **B**, and **C**) all of C_1 symmetries. Table S2 shows the comparison of the total energies and the corresponding dipole moment values for all **LAA** conformers with the B3LYP method by using different basis sets. Calculations using both basis sets predict a lower energy value for the **A** structure as can be seen in Table S2, while the remaining structures have higher energy values. The corresponding structures are given in Figure 1. Table 1 shows a comparison of the calculated geometrical parameters for the **A**, **B**, and **C** structures with the ones observed from X-ray diffraction corresponding to the **LAA**.[5] The calculation predicts that the **A** structure is the most stable according to the experimental results that indicate that only the **A** and **B** structures are present in the crystalline state. The high value of the dipolar moment for the **B** structure could partly explain its experimental stability, as observed by Ledesma et al.[29] for the anti conformer of 2-(2′-furyl)-1*H*-imidazole, Sambrano et al.[30] for the M4 tautomer of 5-methylcytosine and Brandán et al.[31] for the imino-hidroxy tautomer of 1,5-dimethylcytosine. The theoretical values for all structures were compared with the average experimental values reported for the compound by means of the root mean of square deviation (rmsd) values. According to these results, the basis set that best reproduces the theoretical geometrical parameters for **LAA** compound is 6-311++G** for bond lengths and angles, where the mean differences are 0.003, 0.0033, and 0.0031 Å for the **A**, **B**, and **C** structures, respectively, and for the bond angles the values are between 0.34 and 0.59°. In general, our theoretical values are in agreement with the experimental values for **LAA.**[5] In general, it can be seen that the best results are obtained with B3LYP/6-311++G** calculations and the introduction of diffuse functions is essential to have an approximation to the experimental values, especially in the case of the **B** and **C** structures.

The stabilities of the **B** and **C** structures in relation to the **A** structure was investigated by using the electrostatic potential maps.[20,29,32] The molecular electrostatic potential values for all structures by using the 6-31G* and 6-311++G** basis sets are given in Table S3, and Figure 3 shows the electrostatic potential maps for the **A**, **B**, and **C** structures. Note that, for all structures in general, the molecular electrostatic potential values increase according to the size basis set, as can be seen in Table S3. The atomic charges derived from the ESPs (MK)[20] and natural atomic charges were also analyzed and the corresponding values

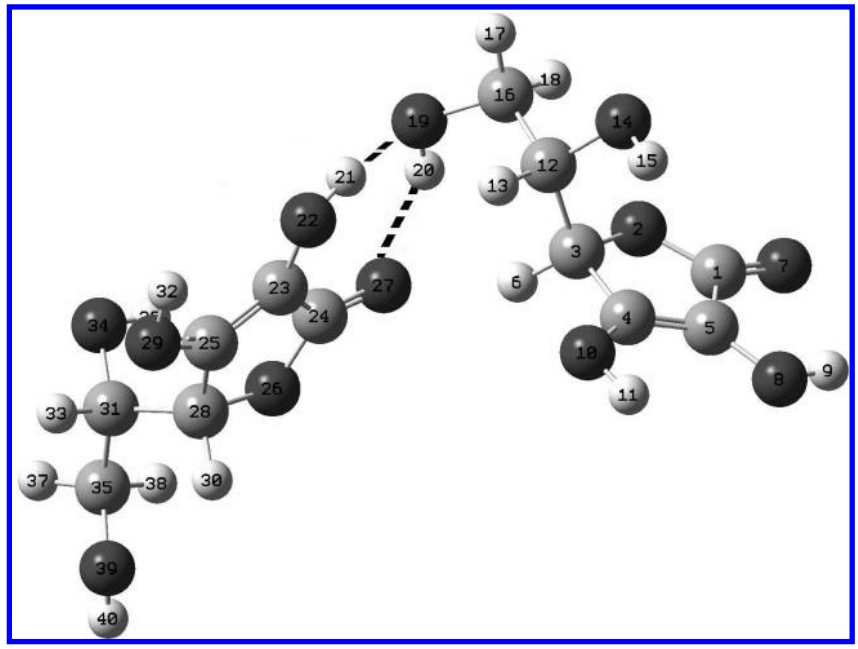

Figure 2. Theoretical structure of dimer L-ascorbic acid. The H-bonding is indicated by dashed lines.

TABLE 1: Comparison of Calculated[a] Geometrical Parameters for All Structures of L-Ascorbic Acid with the Corresponding Experimental Values

	B3LYP/6-31G*			B3LYP/6-311++G**			
parameter	**A**	**B**	**C**	**A**	**B**	**C**	exp[b]
			Bond Lengths (Å)				
C1−O7	1.211	1.210	1.211	1.205	1.204	1.205	1.216
C5–O8	1.358	1.356	1.356	1.356	1.354	1.354	1.361
C4–O10	1.347	1.353	1.353	1.343	1.349	1.350	1.326
C1–O2	1.377	1.371	1.365	1.374	1.367	1.363	1.355
C3–O2	1.450	1.449	1.445	1.449	1.447	1.445	1.444
C12–O14	1.414	1.418	1.416	1.416	1.421	1.418	1.427
C16–O19	1.422	1.419	1.423	1.426	1.423	1.427	1.431
C4–C5	1.343	1.341	1.342	1.340	1.338	1.338	1.338
C1–C5	1.457	1.462	1.463	1.457	1.462	1.464	1.452
C3–C4	1.501	1.501	1.504	1.499	1.499	1.501	1.493
C3–C12	1.540	1.543	1.541	1.537	1.539	1.539	1.521
C12–C16	1.531	1.537	1.526	1.530	1.535	1.525	1.521
rmsd	0.0035	0.0039	0.0034	0.0030	0.0033	0.0031	
			Bond Angles (°)				
C3–O2–C1	109.2	109.5	109.4	109.4	109.7	109.7	109.1
O2–C1–C5	108.7	108.5	108.8	108.5	108.4	108.5	109.5
C1–C5–C4	108.5	108.5	108.3	108.6	108.5	108.4	107.8
C5–C4–C3	109.3	109.3	109.0	109.4	109.4	109.2	109.5
C4–C3–O2	104.1	103.9	104.1	103.9	103.8	103.9	104.0
O2–C1–O7	123.8	124.4	124.7	123.7	124.2	124.5	121.4
O7–C1–C5	127.3	126.9	126.4	127.7	127.3	126.9	129.1
C1–C5–O8	122.2	122.1	121.8	123.1	122.9	122.8	124.6
O8–C5–C4	129.1	129.3	129.7	128.2	128.4	128.6	127.5
C5–C4–O10	131.5	131.4	131.6	131.1	131.1	131.2	133.5
C3–C4–O10	119.1	119.1	119.2	119.4	119.4	119.5	117.1
O2–C3–C12	108.5	110.9	110.2	109.1	110.8	110.7	110.4
C4–C3–C12	114.8	114.2	113.6	109.1	114.9	114.3	114.8
C3–C12–C16	111.4	111.1	111.6	111.5	111.7	111.6	112.7
C3–C12–O14	111.4	112.8	112.3	111.9	112.8	112.7	111.7
O14–C12–C16	110.8	106.0	106.3	110.7	105.7	106.2	106.9
C12–C16–O19	107.7	112.5	107.3	107.6	112.4	107.3	108.0
rmsd	0.40	0.59	0.38	0.50	0.42	0.34	
			Dihedral Angles (°)				
C3–C12–C16-O19	60.8	43.7	60.9	60.4	48.4	61.1	
C3–C12–O14-H15	55.2	–75.4	–68.9	56.9	–79.2	–70.9	
C12–C16–O19-H20	–172.8	–82.3	–164.9	–177.4	–91.4	–168.5	

[a] This work. [b] Reference 5.

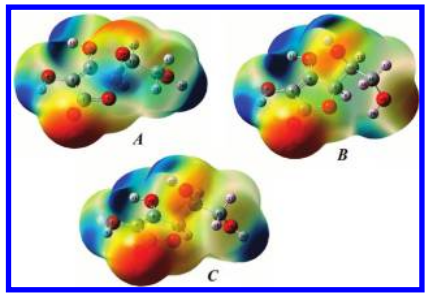

Figure 3. Calculated electrostatic potential surfaces on the molecular surfaces of **A**, **B**, and **C** structures of L-ascorbic acid. Color ranges, in au: from red −0.05 to blue + 0.05. B3LYP functional and 6-31G* basis set. Isodensity value of 0.005.

are given in Tables S4 and S5, respectively. Note that both charges are very different by using the two basis sets. The important factor responsible for the lesser stability of the **C** structure is the electrostatic repulsion between the O2 and O7 and O14 and O10 atoms, whose electrostatic potentials are higher in the **C** structure (Table S3). Hence, a strong red color on these atoms of the lactone ring can be seen in the corresponding Figure 3. On the other hand, in the **B** structure other red color on the O19 atom and moreover a slightly blue color on the H20 atom can be observed, that is, a higher electrostatic potential values in both atoms. The latter observation is justified due to the presence of an observed H-bond, as can be seen later, between the O2 and H20 atoms that probably stabilize this structure. Thus, the **C** structure is more unstable than the corresponding **B**; for this reason, its structure is not experimentally observed despite that the energy value of the **C** structure (Table S2) is slightly higher by using the 6-311++G** basis set than the **B** structure. This fact is justified because with this latter basis set the LP(1)O2 → σ*O19−H20 charge transfer is not observed as can be seen in the following section.

In short, one may conclude that our calculated **A** and **B** structures provide a reliable starting point for the DFT/B3LYP/6-31G* or B3LYP/6-311++G** force fields and frequency calculations.

4.2. NBO and AIM Analyses. The stability of the three **LAA** structures was also investigated by means NBO calculations.[11−14] The second order perturbation energies $E^{(2)}$ (donor → acceptor) that involve the most important delocalization are given in Table S6. After a careful analysis of these results, we found that the contributions of the stabilization energies for the $\Delta ET_{\sigma\rightarrow\sigma^*}$ charge transfers of the **A** structure have lower values than the other delocalizations ($\Delta ET_{LP\rightarrow\sigma^*}$). Also, in the **B** structure only with the B3LYP/6-31G* method, the LP(1)O2 → σ*O19−H20 charge transfer with a magnitude of 4.18 kJ/mol was observed. For this reason, the calculated total energy value favors the **B** structure, as is expected, because in spite of being the most unstable in the gas phase it can experimentally observed in the solid phase.

The molecule structures of LAA have been analyzed by means of Bader's charge electron density, $\rho(r)$ topological analysis.[15] The localization of the bond critical point (BCP) and ring critical point (RCP) in the $\rho(r)$ and the Laplacian values, $\nabla^2\rho(r)$ at these points are important for the characterization of molecular electronic structure in terms of interaction magnitude and nature. This critical point has the typical properties of the closed-shell interaction. That is, the value of $\rho(r)$ is relatively low, the relationship $|\lambda_1|/\lambda_3$ is < 1 and $\nabla^2\rho(r)$ is positive indicating that the interaction is dominated by the charge contraction away from the interatomic surface toward each nucleus. The (ρ) and $\nabla^2\rho(r)$ for the calculated RCP and BCP from the topological property analysis for **A**, **B**, and **C** structures are shown in Table S7. This analysis shows only one RCP in the **A** and **C** structures while in the **B** structure, by using the B3LYP/6-31G* level, one BCP and two RCPs are found. The BCP in the **B** structure is constituted between the O2 and H20 atoms (Table S7). In all the structures, the higher (ρ) and $\nabla^2\rho(r)$ values of the lactone ring, in relation to the other atoms, are significant. Also, the influence of the size basis set on the properties of the ring critical points is notable in the different structures. These results are in agreement with the NBO analysis of the previous section and demonstrate the presence of the H-bond between the O2 and H20 atoms that was not experimentally observed in the solid state. Moreover, this observation is another reason for to justify the stability of this molecule with reference to the **C** structure. On the other hand, the NBO study for the dimer species clearly reveal the energies and occupancies of the main contributions such as, LP(2)O2 → σ*C1═O7 (44.02 kcal/mol), LP(2)O19 → σ*O22−H21 (27.56 kcal/mol), LP(2)O19 → σ*C16−H18 (5.01 kcal/mol), LP(2)O27 → σ*O19−H20 (5.12 kcal/mol), and LP(2)O10 → σ*C4−C5 (32.69 kcal/mol) to the delocalization energy due to the OH−O bonds between both structures. In addition, the four RCPs calculated by means of the AIM analysis corroborate such contributions, as it is expected.

5. Vibrational Analysis

The recorded infrared spectra for the compound in the solid and aqueous solution phases can be seen in Figure 4. As it was mentioned in step 2, the Raman spectrum of L-ascorbic acid was taken from a previous study as reported in ref 4. In this vibrational analysis only the experimentally observed **A** and **B** structures were taken into account. The two **LAA** structures have C_1 symmetries and 54 normal vibration modes, all active in the infrared and Raman spectra. The assignment of the experimental bands to the 54 expected normal vibration modes for **LAA A** and **B** structures were made on the basis of the potential energy distribution (PED) in terms of symmetry coordinates by using the B3LYP/6-31G* data and taking into account the corresponding assignment of related molecules.[4,5,32−36] Table 2 shows the observed frequencies and the assignment for both **LAA** structures considering the previous partial assignments reported for this compound.[4,5] For **A** and **B** structures, the assignment of the vibrational normal modes and the PED based on the 6-31G* basis set are shown in Tables S8 and S9, respectively. Theoretical calculations reproduce the normal wavenumbers for the **A** structure with rmsd initial values of 11.3 and 17.3 cm^{-1} by using the 6-31G* and 6-311++G** basis sets, respectively, and for the **B** structure with rmsd initial values of 15.1 and 17.4 cm^{-1} by using the 6-31G* and 6-311++G** basis sets, respectively. When the SQMFF method is applied by using Pulay's scaling factors, the final RMSDs for both basis sets slightly decrease up to 6.1 and 11.0 cm^{-1} for the **A** structure by using 6-31G* and 6-311++G** basis sets, respectively, and for the **B** structure decrease up to 8.3 and 11.3 cm^{-1} by using 6-31G* and 6-311++G** basis sets, respectively. The best results for both **LAA** structures are obtained with a B3LYP/6-31G* calculation, as is expected because the used scale factors are only defined for this basis set. The SQM force fields for this compound can be obtained at request. Note that the average theoretical infrared spectra between the two **LAA** structures demonstrates an agreement with the experimental spectrum, especially in the 1800 and 900 cm^{-1} region where a higher intensity of the bands associated to the C═O and C═C stretching modes can be seen in Figure 5. On the other hand,

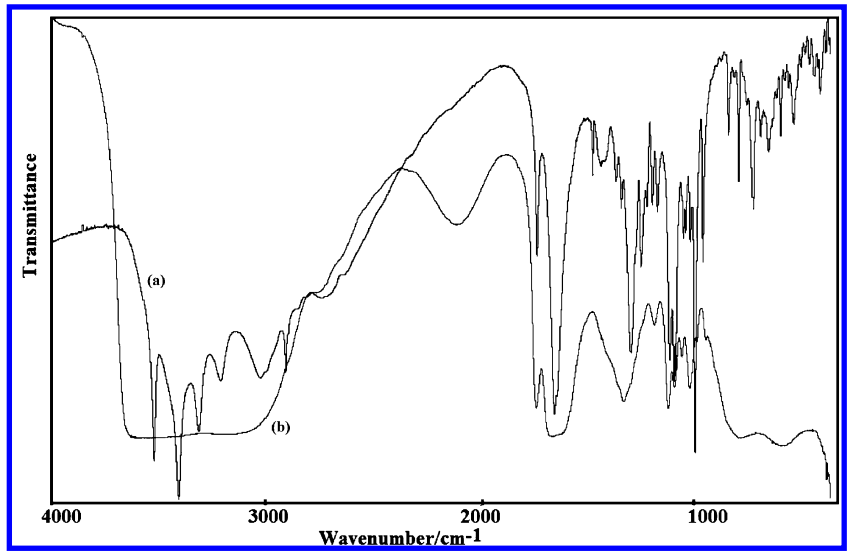

Figure 4. Experimental infrared spectra of L-ascorbic acid: (a) in solid state and, (b) in aqueous solution.

in the IR spectrum in aqueous solution it is possible to observe a notable broad and shifting in the bands related mainly to the OH groups, as it is shown in Figure 4. These shifts, previously observed by Hvoslef and Klaeboe[4] in the Raman spectrum in aqueous solution below 1500 cm^{-1} are attributed to the less defined conformation of the skeletal modes in solution with reference to the solid crystal. The discussion of assignment of the most important groups for the studied compound (see Tables 2, S8, and S9) is presented as follows.

Band Assignments. ***OH Modes.*** For these groups, four stretching modes are expected for the L-ascorbic acid molecule. In accordance to the values reported by Hvoslef and Klaeboe[4] and Paniker et al.[5] these modes are assigned at 3523, 3409, 3316, and 3217 cm^{-1}. The wide band observed between 3600 and 2200 cm^{-1}, and particularly the weak IR band at 2170 cm^{-1} in the IR spectra of the compound in aqueous solution can be attributed to O−H hydrogen bonding formed by the spatial arrangement of molecules in the lattice crystal and in aqueous solution.[2,3,5] The four C−OH scissoring modes for both structures are clearly calculated in the 1400−1100 cm^{-1} region; for this reason, in the **A** structure they are assigned to the IR bands at 1387, 1321, 1274, and 1197 cm^{-1} while in the **B** structure those modes are associated with the IR bands at 1387, 1344, 1258, and 1112 cm^{-1}. In the region of lower wavenumbers, the OH torsion modes are expected for both structures. Some of these modes, as shown in Table 2, appear coupled with other modes of the lactone group.

CH Modes. The group of bands in the 3002−2903 cm^{-1} region in the infrared and Raman spectra of the solid substance can be assigned to the C−H stretching modes. Thus, these modes in the **A** structure are assigned to the Raman bands of medium intensities at 2944 cm^{-1} and at 2916 cm^{-1} in the IR spectrum. For the **B** structure these modes are assigned at 2944 and 2903 cm^{-1}. This assignment is in agreement with that previously reported for this molecule.[4,5] As predicted by the calculations, the C−CH scissoring modes for both structures are easily assigned to the Raman bands at 1344 and 1258 cm^{-1} in the **A** and **B** structures, respectively.

CH_2 Modes. The asymmetric stretching modes of these groups for both structures can be assigned to the Raman bands at 3002 and 2978 cm^{-1}, as in Table 2 is observed, while their corresponding symmetric modes are assigned to the very strong Raman bands at 2916 and 2903 cm^{-1}. The weak Raman band at 1487 and 1450 cm^{-1} are clearly assigned to the scissoring modes corresponding to the **A** and **B** structures, respectively, in agreement with similar compounds containing the CH_2 group[4,5,33] while, as predicted by the calculation, the bands of medium intensities at 1459 and 1387 cm^{-1} are easily assigned to the wagging modes. The expected rocking modes are assigned to the medium intensities bands at 1302 and 1197 cm^{-1} while, for both structures, the twisting modes are associated with the very weak IR band at 924 cm^{-1}. It is important to note that in the two previous assignments[4,5] for this compound all modes related to this group were not clearly detailed and assigned.

Skeletal Modes. According to the values previously reported for **LAA**[4,5] and to our theoretical results, the strong bands at 1753 and 1672 cm^{-1} are mainly associated to the C═O and C═C stretching modes. In the IR spectrum in aqueous solution, the bands associated with these two stretching modes slightly increase their intensities and wavenumbers, as it was also observed in the Raman spectrum in aqueous solution by Hvoslef and Klaeboe,[4] and they have justified this observation because both modes increase the double bond character in aqueous solution. The IR bands at 1302, 1139, 1112, 1076, 1046, and 1026 cm^{-1}, respectively, are associated with the C−O stretching modes, while the C−C stretching modes, as predicted by the calculations, are associated to the IR bands at 1438, 1139, 1067, 990, 821, and 675 cm^{-1} for both structures, as can be seen in Table 2. It can be observed that the band at 1139 cm^{-1} is associated with both C−O and C−C stretching modes of the A and B structures, respectively. The strong IR bands at 1112 and 1026 cm^{-1} are assigned to the C−O stretching modes of the **A** structure lactone ring according to the values reported for the furan molecule by Klots et al.[36] (1181 and 1067 cm^{-1}). For the **B** structure these modes are associated with the bands at 1076 and 1026 cm^{-1}. The splitting of these bands is higher for the **A** structure (86 cm^{-1}) than that of the other one (50 cm^{-1}), as it is expected, according to the difference observed between the values of the corresponding C−O distances presented in Table 1. Taking into consideration the relative position, intensities, and the splitting predicted by calculation, the two lactone ring deformations for both **LAA** molecules are associated with the two pairs of bands observed in the IR and Raman spectra at 591/589 and 568/567 cm^{-1}, respectively. As predict the calculations, the two pairs of bands observed in the Raman spectra, at 138/81 cm^{-1} and at 122/73 cm^{-1} are attributed to the torsion ring modes corresponding to the lactone ring of the two structures. In the 2-(2′-furyl)-4,5-1H-dihydroimidazole mol-

TABLE 2: Observed and Calculated Wavenumbers (cm^{-1}) and Assignments for Monomers and Dimer of L-Ascorbic Acid[a]

IR[b] solid	IR[b] solution	IR[c] solid	Raman[c] solid	Raman[c] solution	assignment[c]	IR[d] solid	Raman[d] solid	SERS[d]	assignment[d]	assignment[b]
3523 s		3535 s			ν O−H	3626 s			ν O−H	ν O−H (**A**, **B**)
3409 vs		3420 s			ν O−H	3410 s			ν O−H	ν O−H (**A**, **B**)
3316 s		3330 s			ν O−H	3315 s			ν O−H	ν O−H (**A**, **B**)
3217 m		3230 m			ν O−H	3216 s			ν O−H	ν O−H (**A**, **B**)
3030 s, br		3050 s, bd			ν O−H	3030 s, br	3004 w	3144 s	ν C−H	ν O−H
			3002 m		ν C−H					νa CH_2 (**B**)
			2978 m		ν C−H					νa CH_2 (**A**)
				2944 m, bd	ν C−H			2949 m	ν C−H	ν C−H (**A**, **B**)
2916 m		2915 m, sp	2916 vs		ν C−H	2917 m	2919 s		ν C−H	ν C−H (**A**), νs CH_2 (**B**)
			2903 vs	2904 m, sp	ν C−H	2907 m			ν C−H	νs CH_2 (**A**), ν C−H (**B**)
2854 w		2860 vw	2866 w	2863 vw			2879 w, sh		ν C−H	ν O−H
2737 w		2740 m, bd			ν O−H					
2641 sh		2650 w								
		2340 w								
1753 m	1758 s	1753 s	1754 w	1762 m, bd	ν C═O	1764 s	1758 w	1788 s	ν C═O	ν C═O (**A**, **B**)
1672 s	1685 s	1670 vs	1667 vs	1693 vs, bd	ν C═C	1675 vvs		1684 vs	ν C═C	ν C═C (**A**, **B**)
1661 sh		1659 vs	1654 vs				1661 vvs			δ CH_2 dim
				1503 w						δ CH_2 dim
		1495 m	1498 m							ν C−C dim
1487 w		1482 w	1487 w	1470 m		1487 m	1484 m		δ CH	δ CH_2 (**A**)
						1468 w				
1459 m		1455 m	1450 w			1463 w	1452 w		δ CH, δ CH_2	wag CH_2 (**A**), δ CH_2 (B)
1438 sh		1435 m								δ HOC (**A**, **B**), ν C−C (**B**)
1387 w		1385 m			δ CH_2	1389 m	1371 w	1386 vvs	wag CH_2 δ COH	δ COH (**A**, **B**), wag CH_2 (**B**)
1363 sh	1353	1362 m	1372 w	1355 w	wag CH_2					δ CCO (**A**, **B**)
			1344 vw		δ C−H					δ CCH (**A**), δ COH (**B**)
1321 m		1320 s	1321 s		δ O−H	1322 m	1323 s		δ CH	δ COH (**A**)
1302 sh		1300 vw	1297 m	1299 m						ρ CH_2 (**A**), ν C−O (**A**, **B**), τw CC_2 (**B**)
1274 s		1270 w		1273 vw		1277 s			ν C−O−C	δ COH (**A**), δ CCH (**B**)
			1258 s				1258 s	1268 s	δ COH	δ COH (**B**)
1246 m		1248 w				1246 m				ρ CH_2 dim
1221 w	1213	1220 m	1226 w	1218 m, bd		1222 s			ν C−C	τw CC_2 (**A**)
1197 w		1197 m	1200 m			1199 s	1193 w		ν C−C	δ COH (**A**), ρ CH_2 (**B**)
1139	1148	1138 s	1131 vs	1150 m	ν C−O	1142 vs			ν C−O	ν C−O (**A**), ν C−C (**B**)
1120	1120	1118				s1121 vs				ν C−O dim
1112 s		1110 s	1114 vw	1119 w	ν C−C	1113 vs	1113 s		ν C−O−C	ν C−O (**A**), δ COH (**B**)
1076 w	1084	1074 m		1087 vw		1077 m	1081 w		ν C−O−C	ν C−O (**A**, **B**)
1067 w		1065 m	1066 m	1052 m		1055 m			δ COH	ν C−C (**A**), ν C−O (**B**)
1046 sh	1047	1042 w	1039 vw			1046 m	1048 m		δ COH	ν C−O (**A**)
1026 vs		1025 s	1026 s	1022 w		1027 vvs			δ COH	ν C−O (**A**, **B**)
990 m		988 s	993 w	981 vw		990 s	984 w	960 m		ν C−C (**A**, **B**)
924 vw				937 m, bd						τw CH_2 (**A**, **B**)
870		869 m	872 m	873 m, bd		871 w	871 m	872 m	ν C−C	ν C−C dim
821 w		820 m	822 s	826 vs		821 m	823 m			ν C−C (**A**, **B**)
				797 vw						γ C−C (**B**)
783 vw								782 m	τ (OH)	γ C−C (**A**)
756		756 s	742 w	768 vw		757 s	742 sh			τ (OH)ip dim
722		721 m, bd				722 w				γ C═O dim
		711 vw	711 m							γ C═O (**A**, **B**)
			694 w	697 s			693 m			τw CH_2 dim, β C═O dim
686 w						686 w				β C═O (**A**, **B**)
675 sh		675 m, bd								ν C−C (**A**), ν C−O (**B**)
649				664 m						τ (OH)op dim
628		629 m	629 s	633 s			621 s			$\beta$$R_1$ dim
591 w			589 s	589 m			581 w			$\beta$$R_1$ (**A**, **B**)
568 w		565 m	567 s	565 w, bd			564 m	562 s	τ (OH), ν C−C	δ OCH (**A**), $\beta$$R_2$ (**A**, **B**), γ C−O (**B**)
496 w		494 vw	490 w	488 w						δ CCO (**B**)
473 w		473 w	477 m				468 w			δ CCO (**A**)
449 w		448 m	448 s	445 m, bd			452 w	455 s	β C−O	ρ CC_2 (**A**), Wag CC_2 (**B**)
				396 w, bd						τ (OH) (**A**, **B**)
		366 s	363 m							τ (OH) (**A**, **B**)
		350 s								τ (OH) (**A**)
		340 w	345 m							γ C−O (**A**, **B**), τ (OH) (**B**)
		292 w	295 m	305 w, bd						β C−O (**A**, **B**)
			273 w							Wag CC_2 (**A**), ρ CC_2 (**B**)
			259 m							τ (OH) dim
		238 m								τ (OH) dim
			223 m							β C−O (**A**, **B**), τ (OH) (**A**)
			208 m							δ CCC (**A**, **B**)
			180 w							γ C−C dim
			163 m							τ CCCO dim
			148 m							γ C−O (**A**), δ OCH (**B**)
			138 m							$\tau$$R_1$ (**B**)
			122 w							$\tau$$R_1$ (**A**)
			113 w							τ CCCO (**A**)
			91 m							τ CCCO (**B**)
			81 s							$\tau$$R_2$ (**B**)
			73 s							$\tau$$R_2$ (**A**)
			43 vw							τw Ring (**A**, **B**)

[a] ν, stretching; δ, scissoring; wag, wagging; γ, out- of plane deformation; β, in- plane deformation; ρ, rocking; τ, torsion, τw, twisting; *a*, antisymmetric; *s*, symmetric; R, ring, s, strong; m, medium; w, weak; v, very; sh, shoulder; br, broad; dim, dimer. [b] This work. [c] From ref 4. [d] From ref 5.

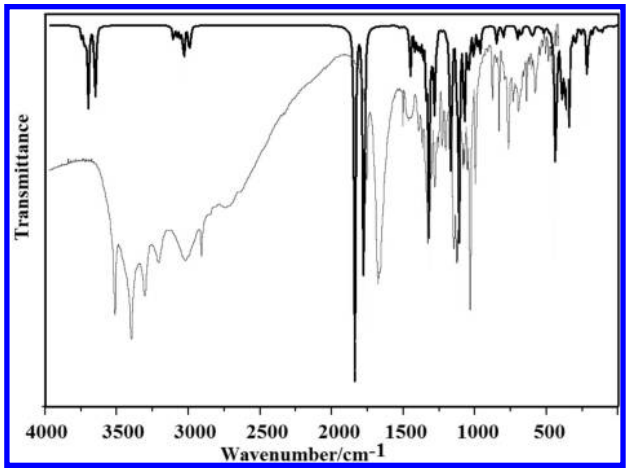

Figure 5. Comparison between the refined average calculated (upper) and experimental infrared spectra (bottom) of L-ascorbic acid. The calculated spectrum was obtained from B3LYP/6-31G* using average frequencies and intensities for both structures.

ecule,[35] the torsion ring modes can be seen at 304 and 172 cm^{-1}. Hence, we can see that the effect of the carboxyl and hydroxyl groups on the furane ring is the displacement of these vibrational modes toward lower frequencies. The Raman and IR bands at 711 and 686 cm^{-1} can be associated with the out-of-plane and in-plane C═O deformation mode, respectively, while the weak IR band at 568 cm^{-1} and the Raman bands of medium intensities at 345 and 148 cm^{-1} could be assigned to the out-of-plane C−O deformation modes of both structures. The corresponding in-plane C−O deformation modes for both structures are clearly assigned to the Raman bands of medium intensities at 295 and 223 cm^{-1}. In this compound, both structures are present in the solid phase; for this reason, a comparison between the average calculated infrared spectra (from the B3LYP/6-31G* level for the **A** and **B** structures) by using average wavenumbers and intensities with the corresponding experimental ones demonstrate a good correlation (Figure 5). These results are supported by the highly strong bands at 1858, 1793, 1341, 1191, 1130, and 1091 cm^{-1} in the calculated IR spectrum for the **A** structure and at 1861, 1800, 1337, 1185, 1146, and 1129 cm^{-1} for the **B** structure, also by the intense bands, only observed in the latter structure at lower wavenumbers (364 and 335 cm^{-1}) due to their intensities that slightly decrease when the average infrared spectra are calculated so, in this way, the resulting spectrum is approximately similar to the experimental one.

Dimer Modes. The optimized dimer **LAA** structure by using the B3LYP/6-31G* level has C_1 symmetry and 114 normal vibration modes, all active in the infrared and Raman spectra. The assignment of the experimental bands to the 114 expected normal vibration modes were made by means of the *GaussView* program[27] by analyzing the nature of the vibrations. In this case, we presented in Table 2 only the bands not assigned to the **A** and **B** monomers. Thus, the shoulder at 1661 cm^{-1} and the very strong Raman band at 1654 cm^{-1} are associated with the CH_2 scissoring modes because these vibration modes are predicted by calculation in the 1550−1534 cm^{-1} region. The IR and Raman bands of medium intensities at 1495 and 1498 cm^{-1}, respectively, and the band at 870 cm^{-1} are assigned to the C−C stretching modes, and the band at 1246 cm^{-1} is associated with the CH_2 rocking mode. The C−O stretching is calculated at 1131 cm^{-1}; for this reason, the band at 1120 cm^{-1} is assigned to this vibration mode. In the region between 770 and 620 cm^{-1} the calculations clearly predict the in-phase OH torsion (798 cm^{-1}) and the out-of-plane C═O deformation modes (728 and 723 cm^{-1}); thus, the IR bands at 756 and 722 cm^{-1} are assigned respectively to those modes. The group of bands between 697 and 628 cm^{-1} in the infrared and Raman spectra of the solid substance can be assigned, as indicated in Table 2, to the CH_2 twisting (699 cm^{-1}), to the in-plane C═O deformation (691 cm^{-1}), to the out-of-phase OH torsion (664 cm^{-1}), and to the lactone ring deformation modes (695, 627, and 620 cm^{-1}). Finally, the Raman bands at 259, 223, 180, and 163 cm^{-1} and the IR bands at 238 cm^{-1} are assigned, as predicted by calculations, to the OH torsion (242 cm^{-1}), to the in-the plane C−O deformation (224 cm^{-1}), to the out-of-plane C−O deformation modes (211 and 196 cm^{-1}), and to the CCCO torsion modes (168 cm^{-1}), respectively.

TABLE 3: Scaled Force Constants for A and B Structures of L-Ascorbic Acid[a]

	B3LYP/6-31G*		B3LYP/6-311++G**	
description	**A**	**B**	**A**	**B**
$f(\nu O-H)$	7.11	7.11	7.43	7.45
$f(\nu C-C)$	4.24	4.18	4.17	4.10
$f(\nu C=C)$	8.47	8.54	8.37	8.44
$f(\nu C=O)$	12.32	12.40	12.02	12.10
$f(\nu C-H)$	4.86	4.71	4.79	4.67
$f(\nu CH_2)$	4.65	4.85	4.64	4.80
$f(\nu C-O)$	4.36	4.46	4.25	4.35
$f(\delta CH_2)$	0.84	0.81	0.80	0.77
f(wag CH_2)	0.78	0.75	0.77	0.74
$f(\beta R)$	0.31	0.31	0.27	0.32
$f(\tau R)$	0.29	0.20	0.20	0.20

[a] Units in mdyn $Å^{-1}$ for stretching and mdyn Å rad^{-2} for angle deformations.

6. Force Field

For the L-ascorbic acid, the corresponding force constants were estimated by using Pulay et al.[24−26] scaling procedure as mentioned before. The force constants expressed in terms of simple valence internal coordinates were calculated from the corresponding scaled force fields by using the MOLVIB program.[21,22] It is interesting to compare the principal force constants calculated at the B3LYP/6-31G* level, which were collected in Table 3, with those obtained by using the B3LYP/6-311++G** combination. The calculated force constants values for both structures by using the different methods are slightly different between them. In some cases these variations are in accordance with the observed changes in the geometrical parameters when the size basis set increases, while in other cases, as in the $f(\nu O-H)$, $f(\nu C=O)$, $f(\nu C=C)$, and $f(\nu CH_2)$ force constants values, the highest variations in the calculated wavenumbers when the size basis set increases justify such differences.

7. Conclusions

The main conclusions of the present paper are the following: (1) We have characterized the substance by IR spectroscopic techniques in the solid state and in aqueous solution phases. (2) We have determined the theoretical molecular structures of L-ascorbic acid by the B3LYP/6-31G* and B3LYP/6-311++G** methods and calculations that suggest the existence of the **A** and **B** stable structures in the gas phase as it was observed in the solid state. (3) The stability of the **B** structure of L-ascorbic acid was justified by means of electrostatic potentials, NBO, and AIM analyses. (4) The average calculated harmonic vibrational wavenumbers for the **A** and **B** structures of L-ascorbic acid is consistent with the observed infrared spectrum

in the solid state. (5) The presence of both conformers in the solid of L-ascorbic acid was detected in the IR spectrum, and a complete assignment of the vibrational modes was accomplished. (6) The SQM force fields were obtained for the **A** and **B** structures of L-ascorbic acid after adjusting the theoretically obtained force constants in order to minimize the difference between the observed and calculated wavenumbers.

Acknowledgment. This work was subsidized with grants from CIUNT (Consejo de Investigaciones, Universidad Nacional de Tucumán), and CONICET (Consejo Nacional de Investigaciones Científicas y Técnicas, R. Argentina). The authors thank Professor Tom Sundius for his permission to use MOLVIB.

Supporting Information Available: Table S1 includes the definition of Natural Internal Coordinates, Table S2 includes the calculated total energy (*E*) and dipolar moments for all theoretical stable structures of L-ascorbic acid. Table S3 includes the calculated molecular electrostatic potential (atomic units) of all theoretical stable structures, Table S4 includes the MK charges for all theoretical stable structures, Table S5 includes the natural charges for all theoretical stable structures, Table S6 includes the main delocalization energy (in kJ/mol) for all theoretical stable structures of L-ascorbic acid. Table S7 includes an analysis of the Ring Critical Point (RCP) for all theoretical stable structures of L-ascorbic acid at different theory levels. Table S8 includes the observed and calculated wavenumbers (cm^{-1}) and assignments for A structure of L-ascorbic acid while Table S9 includes the observed and calculated wavenumbers (cm^{-1}) and assignments for B structure of L-ascorbic acid. This information is available free of charge via the Internet at http://pubs.acs.org.

References and Notes

(1) Paasch, S.; Salzer, R. *Anal Bioanal Chem.* **2004**, *380*, 734.
(2) Hvoslef, J. *Acta Crystallogr.* **1968**, *B24*, 23.
(3) Hvoslef, J. *Acta Crystallogr.* **1968**, *B24*, 1431.
(4) Hvoslef, J.; Klaeboe, P. *Acta Chem. Scand.* **1971**, *25*, 3043.
(5) Panicker, C. Y.; Varghese, H. T.; Philip, D. *Spectrochim. Acta Part A* **2006**, *65*, 802.
(6) Zatikyan, A. I.; Kazoyan, E. A.; Bonora, S.; Markaryan, Sh. A. *J. Appl. Spectrosc.* **2008**, *75* (5), 664.
(7) Hong, Y.; Irudayaraj, J. *J. Pharm. Pharmacol.* **2002**, *54* (9), 1247.
(8) Rauhut, G.; Pulay, P. *J. Phys. Chem.* **1995**, *99*, 3093.
(9) Rauhut, G.; Pulay, P. *J. Phys. Chem.* **1995**, *99*, 1457.
(10) Kalincsák, F.; Pongor, G. *Spectrochim. Acta A* **2002**, *58*, 999.
(11) Reed, A. E.; Curtis, L. A.; Weinhold, F. *Chem. Rev.* **1988**, *88* (6), 899.
(12) Foster, J. P.; Weinhold, F. *J. Am. Chem. Soc.* **1980**, *102*, 7211.
(13) Reed, A. E.; Weinhold, F. *J. Chem. Phys.* **1985**, *83*, 1736.
(14) Glendening, E. D.; Badenhoop, J. K.; Reed, A. D.; Carpenter, J. E.; Weinhold, F. *NBO 3.1*; Theoretical Chemistry Institute, University of Wisconsin; Madison, WI, 1996.
(15) Bader, R. F. W. *Atoms in Molecules, A Quantum Theory*; Oxford University Press: Oxford, 1990; ISBN: 0198558651.
(16) Biegler-Köning, F.; Schönbohm, J.; Bayles, D. AIM2000; A Program to Analyze and Visualize Atoms in Molecules. *J. Comput. Chem.* **2001**, *22*, 545.
(17) Becke, A. D. *Phys. Rev.* **1988**, *A38*, 3098.
(18) Lee, C.; Yang, W.; Parr, R. G. *Phys. Rev.* **1988**, *B41*, 785.
(19) Frisch, M. J.; Trucks, G. W.; Schlegel, H. B.; Scuseria, G. E.; Robb, M. A.; Cheeseman, J. R.; Montgomery J. A., Jr.; Vreven, T.; Kudin, K. N.; Burant, J. C.; Millam, J. M.; Iyengar, S. S.; Tomasi, J.; Barone, V.; Mennucci, B.; Cossi, M.; Scalmani, G.; Rega, N.; Petersson, G. A.; Nakatsuji, H.; Hada, M.; Ehara, M.; Toyota, K.; Fukuda, R.; Hasegawa, J.; Ishida, M.; Nakajima, T.; Honda, Y.; Kitao, O.; Nakai, H.; Klene, M.; Li, X.; Knox, J. E.; Hratchian, H. P.; Cross, J. B.; Bakken, V.; Adamo, C.; Jaramillo, J.; Gomperts, R.; Stratmann, R. E.; Yazyev, O.; Austin, A. J.; Cammi, R.; Pomelli, C.; Ochterski, J. W.; Ayala, P. Y.; Morokuma, K.; Voth, G. A.; Salvador, P.; Dannenberg, J. J.; Zakrzewski, V. G.; Dapprich, S.; Daniels, A. D.; Strain, M. C.; Farkas, O.; Malick, D. K.; Rabuck, A. D.; Raghavachari, K.; Foresman, J. B.; Ortiz, J. V.; Cui, Q.; Baboul, A. G.; Clifford, S.; Cioslowski, J.; Stefanov, B. B.; Liu, G.; Liashenko, A.; Piskorz, P.; Komaromi, I.; Martin, R. L.; Fox, D. J.; Keith, T.; Al.Laham, M. A.; Peng, C. Y.; Nanayakkara, A.; Challacombe, M.; Gill, P. M. W.; Johnson, B.; Chen, W.; Wong, M. W.; Gonzalez, C.; Pople, J. A. Gaussian 03, Revision B.01; Gaussian, Inc.: Wallingford CT, 2004.
(20) Besler, B. H.; Merz, K. M., Jr.; Kollman, P. A. *J. Comput. Chem.* **1990**, *11*, 431.
(21) Sundius, T. *J. Mol. Struct.* **1990**, *218*, 321.
(22) Sundius, T. *Vib. Spectrosc* **2002**, *29*, 89.
(23) Fogarasi, G.; Császár, A. G. *Spectrochim. Acta* **1988**, *44A* (11), 1067.
(24) Pulay, P.; Fogarasi, G.; Pang, F.; Boggs, E. *J. Am. Chem. Soc.* **1979**, *101* (10), 2550.
(25) Pulay, P.; Fogarasi, G.; Pongor, G.; Boggs, J. E.; Vargha, A. *J. Am. Chem. Soc.* **1983**, *105*, 7037.
(26) (a) Rauhut, G.; Pulay, P. *J. Phys. Chem.* **1995**, *99*, 3093. (b) Rauhut, G.; Pulay, P. *J. Phys. Chem.* **1995**, *99*, 14572.
(27) Nielsen, A. B.; Holder, A. J. *GaussView 3.0, User's Reference*: Gaussian Inc.: Pittsburgh, PA, 2000−2003.
(28) Boys, S. F.; Bernardi, F. *Mol. Phys.* **1973**, *19*, 553.
(29) Ledesma, A. E.; Brandán, S. A.; Zinczuk, J.; Piro, O.; López, J. J.; Ben Altabef, A. *J. Phys. Chem. Org.* **2008**, *21* (12), 1086.
(30) Sambrano, J. R.; de Souza, A. R.; Queralt, J. J.; Oliva, M.; Andrés, J. *Chem. Phys.* **2001**, *264*, 333.
(31) Brandán, S. A.; Benzal, G.; García-Ramos, J. V.; Otero, J. C.; Ben Altabef, A. *Vib. Spect.* **2008**, *46*, 89.
(32) Ledesma, A. E.; Zinczuk, J.; Ben Altabef, A.; López-González, J. J.; Brandán, S. A. *J. Raman Spectrosc.* **2009**, *40* (8), 1004.
(33) Ledesma, A E.; Zinczuk, J.; López González, J. J.; Ben Altabef, A.; Brandán, S. A. *J. Mol. Struct.* **2009**, *924−926*, 322.
(34) Ledesma, A. E.; Zinczuk, A. E.; López González, J. J.; Ben Altabef, A.; Brandán, S. A. *J. Raman Spectrosc.* **2009**, DOI: 10.1002/jrs.2482.
(35) Zinczuk, J.; Ledesma, A. E.; Brandán, S. A.; Piro, O. E.; López-González, J. J.; Ben Altabef, A. *J. Phys. Org. Chem.* **2009**, *21*, 1.
(36) Klots, T. D.; Chirrido, R. D.; Steele, W. V. *Spectrochim. Acta A* **1994**, *50*, 765.

JP912251G